JOM, Vol. 77, No. 10, 2025
https://doi.org/10.1007/s11837-025-07508-7

Influence of the Manufacturing Process and Dynamic Testing on the Residual Stress State of Additively Manufactured Ti-6Al-4V Lattice Structure Specimens

LENA BURGER ,[1,3,5] HEINZ PALKOWSKI,[2,6] SVEN ULRICH,[3,7] and HADI MOZAFFARI-JOVEIN[1,4,8]

1.—Institute for Materials Science and Engineering (IWAT), Furtwangen University Campus Tuttlingen, Kronenstraße 16, 78532 Tuttlingen, Germany. 2.—Institute of Metallurgy, Clausthal University of Technology, Robert-Koch-Straße 42, 38678 Clausthal-Zellerfeld, Germany. 3.—Institute for Applied Materials – Applied Materials Physics (IAM-AWP), Karlsruhe Institute of Technology, Hermann-von-Helmholtz-Platz 1, 76021 Karlsruhe, Germany. 4.—Department of Microsystems Engineering, University of Freiburg, Georges-Köhler-Allee 103, 79110 Freiburg, Germany. 5.—e-mail: lena.burger@hs-furtwangen.de. 6.—e-mail: heinz.palkowski@tu-clausthal.de. 7.—e-mail: sven.ulrich@kit.edu. 8.—e-mail: hadi.mozaffari@hs-furtwangen.de

With time, the benefits of additive manufacturing have become firmly established in the domain of medical technology. The high degree of design freedom and precision afforded by additive manufacturing enables the production of implant components that are precisely tailored to individual requirements and based on patient-specific data. In addition to the advantages, the production of such components presents process-related material science challenges. One such challenge of this manufacturing process is the residual stresses due to the occurring phase transformation during the rapid process-related cooling rates. These stresses can lead to component deformation and impair the mechanical load-bearing capacity of the component, leading to accelerated fatigue. This aim of this study is to analyse the various influences of manufacturing and machining processes such as heat-treatment or application-related stress on the residual stress state of additively manufactured components based on titanium alloys.

INTRODUCTION

In medical technology, implants are undergoing substantial development across a range of disciplines, driven by continuous advancements in research. This evolution is evident in the emergence of novel applications, materials, processes, and design concepts. Among the most notable advancements is additive manufacturing, a process-based approach that facilitates the customization of implants to a remarkable degree, allowing for precise adaptation to individual patient needs, even beyond standard sizes.[1] The generative manufacturing method enables the realization of geometries that were previously unfeasible using subtractive manufacturing processes, even at the smallest scales. For instance, it is possible to add roughness to specific areas of an implant or to place open-pored or lattice structures on a bulk material to allow blood vessels and bone tissue to grow in. Furthermore, these lattice structures can serve as a storage area for medication. In this regard, it is imperative to equip these lattice structures with a drug-delivery component, thereby facilitating an on-site effect by incorporating antibacterial or antimicrobial agents, such as magnesium, or bone-building substances, like hydroxyapatite, directly in areas with limited vascularization.

Laser powder bed fusion (LPBF) is a generative manufacturing process in which metallic powder is applied in layers using a blade and partially melted using a laser beam.[2–4] The process is based on a

(Received March 29, 2025; accepted May 19, 2025; published online July 8, 2025)

previously constructed CAD model (computer-aided design), which is divided into individual layers.[5,6] The process commences with the application of a predetermined, thin layer of powder onto a building platform, where a laser beam melts the powder in a localized manner, resulting in the formation of a solid layer of material. After solidification, the platform is lowered, and a new layer of powder is applied. This cycle is repeated until the component is fully constructed.

It is imperative to note that the process is conducted in an argon or other inert gas atmosphere to prevent oxidation during manufacturing.[2–4] The process of selective laser beam melting involves extremely rapid cooling of the laser-generated micro-melts, with cooling rates ranging from 10^3 K/s to 10^6 K/s being typical.[7,8] This rapid cooling can result in various forms of deformation, including elastic deformations, on both micro and macro scales, caused by a significant number of residual stresses.[8] Residual stresses that arise during the additive manufacturing process can be attributed to phase transformation occurring at the microstructural level. Instead of a solidification under equilibrium conditions, a diffusionless martensitic transformation occurs because of the previously referenced rapid cooling rates. The resulting mainly martensite phase with a few prior β-grains is characterised by internal residual stresses because of the changed c/a axis ratios of the martensitic crystal lattice. These internal residual stresses can manifest, for example, in geometric shape changes, with more difficult adjustment of the component properties' brittle behaviour under mechanical and dynamic loads.[9] In addition, the dimensional accuracy of the manufactured components changes, so that increased effort is required for reworking. Residual stresses caused by the process-related phase transformation can be eliminated by reworking.[10–12] One way of achieving this is by subsequent heat treatment. In the case of the titanium-based alloy used in this study, this means that diffusion processes are activated in the component at a specified temperature and time, resulting in a transformation of the martensitic microstructure into the stable mixed phases α and β, which have significantly lower residual stresses.

Titanium (Ti) and its alloys are utilized in a variety of industries such as biomedical and aerospace engineering because of their exceptional combination of low density (approximately 4.5 g/cm^3), high specific strength (approximately 53–220 MPa cm^3/g, depending on the alloy), excellent biocompatibility, excellent corrosion resistance, and high fatigue strength.[13] Pure titanium, classified as an allotrope material, crystallizes in a high-temperature body-centred cubic (bcc) β-phase and reversibly transforms into a low-temperature hexagonal close-packed (hcp) α-phase at the β-transus temperature of 882°C.[13] The stability of both phases can be enhanced by the addition of different alloying elements such as aluminium (Al) or vanadium (V). The resulting microstructure can be tailored by varying the quantity of alloying elements, thereby enabling the control of the amount and distribution of the two phases.[9] This process facilitates the creation of titanium alloys that exhibit either an α-type, β-type, or an α + β-type microstructure, thus allowing for the customization of material properties to meet specific requirements.[13] The alloy utilized for the ensuing investigations comprises a titanium-based alloy with alloying elements Al and V. The Al present in the alloy with 6 wt.% exerts a stabilizing effect on the α-phase of the alloy, consequently leading to an elevated transus temperature. V, accounting for 4 wt.% of the alloy, exerts an isomorphous stabilizing effect on the β-phase of the alloy, thereby increasing the existence range of the β-phase.[13] The concurrent presence of both elements in an alloy leads to an expansion of the phase coexistence range of the α- and β-phase.[13] In the cooled cast state, this alloy exhibits a lamellar duplex structure of α and β lamellae at the microstructural level compared to commercially pure (cp) Ti.[13] This type of microstructure is frequently called a basket-weave microstructure because of its cluster-like arrangement of lamellar α areas in former β grains.[13] The orientation of these α cluster areas is aligned with the 12 sliding systems of the cubic space-centred β-cell.[13]

During the additive processing of the (α + β) alloy Ti-6Al-4V, no equilibrium solidification of the melts occurs because of the high cooling rates of the micro-melts. Consequently, no basket-weave microstructure is formed from former β-grains and α-lamellae. Martensitic solidification occurs from the melt and the formation of an α′/α phase.[14]

EXPERIMENTAL DETAILS

Materials and Sample Preparation

The Ti-6Al-4V metal powder from AP&C was used for the additive manufacturing of the samples. The chemical composition of the powder, which was measured with energy-dispersive X-ray spectroscopy (EDX), is presented in Table I below. The elements oxygen (O) and carbon (C) were not considered because of their low molecular mass and the associated lack of scientific clarity.

The samples were produced using the laser powder bed fusion (LPBF) process with a Concept Laser Mlab cusing 100 R. The specimens for dynamic testing have a solid base plate and a body-centred cubic lattice cell (bcc) in three rows

Table I. Chemical composition of the used metal powder Ti-6Al-4V (wt.%)

Material	Ti	Al	V
Ti-6Al-4V	Bal.	6.09	3.73

and two layers. The precise dimensions of the specimens are illustrated in Fig. 1 below.

The samples were produced under controlled argon (Ar) atmosphere. A laser operating at 95 W with a scanning speed of 900 mm/s was employed to ensure efficient material processing. The hatch distance was meticulously calibrated to 100 μm to ensure optimal overlap of the melted areas. Furthermore, a layer thickness of 25 μm was employed, enabling high-resolution and intricate detail in the manufactured parts. These processing parameters yielded a calculated energy density of about 42 J/mm^3, which is pivotal for the microstructure and properties of the additively manufactured components. After the manufacturing process, the surplus powder that remains within the open-pored grid structures is eliminated using compressed air and ultrasonic cleaning in an ethanol bath.

The following investigations are based on two basic sample conditions. First, samples that remained in their original as-manufactured condition after production and were not subjected to any further treatment were analyzed. The second group of specimens consisted of specimens that were heat-treated after production. These were treated at 800°C for 2 h in a controlled Ar atmosphere and then cooled in a controlled manner in the furnace.

ITs minimize potential disturbances to the load transmission during the test; it is necessary to prepare the surface that will be in contact with the indenter during the dynamic test. For this purpose, the specimens were manually ground with silicon carbide (SiC) paper to 2500 grit. The specimens were then pre-polished with a 9-μm and 3-μm diamond suspension and finally polished with a 0.06-μm suspension. The microstructure visualization specimens were prepared similarly and then etched according to Kroll (10 vol.% HF and 5 vol.% HNO_3) to make the microstructure visible. Subsequently, the microstructure of the two ground states was documented optically at multiple points on the sample using an optical microscope.

Dynamic Testing

The fatigue tests were executed in a dynamic displacement-controlled manner. The specimen was supported on surfaces that were not equipped with elementary cells. During the test, the cells were aligned downward. The specimen was subjected to a linear load with a radius of 1 mm in the centre during the test. As illustrated in Fig. 2, the installation condition of the sample was as follows:

The experimental protocol consists of subjecting the samples to sinusoidal compressive loads within the pressure threshold range. However, the specimens are not fully unloaded between cycles but rather are reduced to a small compressive load before being loaded again. Samples that have reached 10^7 load cycles are designated as "runners," and the frequency set for this is 2 Hz. For the initial tests, this selected frequency is approximately half the load frequency resulting from the period duration T for normal walking or stumbling according to Bergman et al.[15] Since the tests are displacement-controlled, travel distances for the indenter are selected based on the elastic deformation behaviour of the Ti-6Al-4V alloy used. These should simulate a reversible elastic deformation of the sample. Based on the results, the travel distance is increased or decreased for the following samples. The outcomes of these experiments are meticulously documented in a Wöhler diagram.

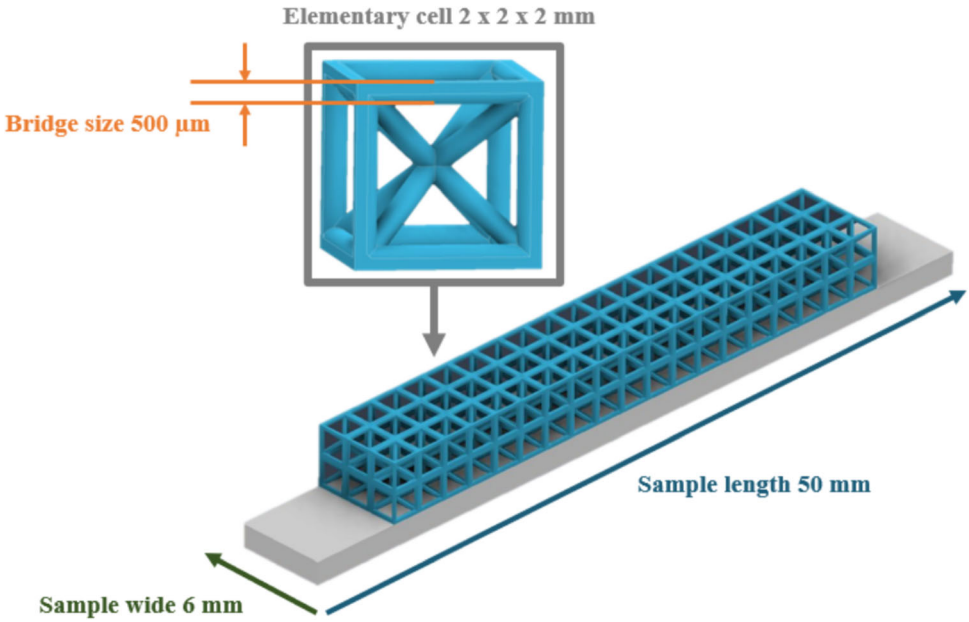

Fig. 1. Dimensions of the specimens for dynamic fatigue testing.

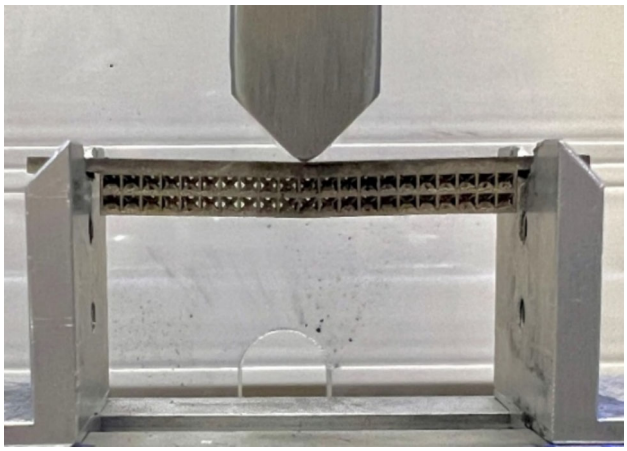

Fig. 2. Installation condition of the specimens for displacement-controlled dynamic fatigue testing with 3-point contact.

X-ray Diffraction (XRD)

The near surface residual stress state of the samples is determined through the X-ray diffractometer (XRD, Bruker, D8 Discovery) using the $d \sim \sin^2\psi$ method. The influence of various factors, such as heat treatment conditions, sample preparation and dynamic testing, can be investigated.[16] The measurement is conducted using monochromatic Cu-Kα radiation at a 40 kV voltage. The residual stresses (RS) present in the near-surface region can be quantified by measuring the lattice expansion with an X-ray diffractometer.[17,18] The measurement of the lattice strain compared to the stress-free mesh plane spacing makes it possible to quantify the RS.[19] The measurement of the lattice plane spacing is based on Bragg's equation.[19] For this purpose, the shift of the reflection peak of the sample is measured at different rotation and tilt angles.

RESULTS AND DISCUSSION

Microstructure of Additively Manufactured Ti-6Al-4V

As illustrated in Fig. 4, the additively manufactured Ti-6Al-4V samples were etched according to Kroll at varying magnification levels to reveal their microstructural phase composition.

The plane of interest, designated as the X-Y plane, corresponds to the build-up plane of the samples in the z-direction. The upper row of images, labeled (a) and (b), show the sample in its untreated as-built state. The lower row of images (c) and (d), on the other hand, showcases the microstructure after undergoing a subsequent heat treatment at 800°C for 2 h in an Ar atmosphere and following controlled furnace cooling.

The as-built sample exhibits a needle-like martensitic microstructure consisting of the hexagonal (hcp) α-phase and martensitic α'-phase. The α'-phase manifests itself in the micrographs in the mainly needle-like form. The needles, with a length of several tens of micrometres, are observed to be grouped in clusters with varying orientations. The microstructure exhibits no evidence of a β-phase. The prevailing theory posits that this phase should form from the melt in conjunction with the alpha phase during equilibrium solidification. Moreover, the alloy utilized contains 4 wt.% of the β-phase isomorph stabilizing element vanadium (V).[20]

In contrast, the sample that underwent a treatment at 800°C/2 h of heat exposure demonstrates a substantially coarser microstructure. In this specimen, the presence of a basket-weave-like structure consisting of the α-phase is even more recognizable, as indicated by the white arrow in Fig. 3c). Additionally, the presence of β grains is observed, situated between the α structures. The two phases are present in hexagonal close packing (α-phase, hcp) and in a body-centred cubic structure (β-phase, bcc). The observations indicate that a phase transformation takes place during the heat treatment process. This phenomenon can be represented by the following reaction:[21]

$$\alpha' \rightarrow \alpha\,(\mathrm{hcp}) + \beta(\mathrm{bcc})$$

The application of heat treatment results in a substantial enhancement of the microstructure, as evidenced by the observations presented in Fig. 3d. The length dimensions of the α phase remain largely unchanged compared to the as-built α'-phase. However, the needles exhibit a notable increase in width, thereby acquiring a significantly stronger lamellar character.

Dynamic Fatigue Testing of Additively Manufactured and Heat-Treated Specimens

The evaluation of microstructural images has shown that the process of selective laser beam melting results in the formation of different microstructures from those in conventionally produced and processed titanium alloys. The locally very high cooling rates in the micro-melts lead to non-equilibrium solidification and thus to the formation of a martensitic α' phase. This solidification process results in process-related high RS. These have a significant influence on the mechanical properties, such as the fatigue resistance of the manufactured components. The influence of RS is particularly visible here in the form of premature failure.

The influence of cooling conditions, microstructure, and RS on the dynamic fatigue resistance of additively manufactured lattice structures is illustrated by the Wöhler curves (see Fig. 4). The orange diamonds represent the points of the as-built Wöhler tests, while the blue points indicate the results of a subsequent heat treatment at 800°C/2 h in an Ar atmosphere and controlled furnace cooling. The fatigue strength of the as-built Ti-6Al-4V samples is nearly half that of the heat-treated condition. The predicted fatigue strength is attained

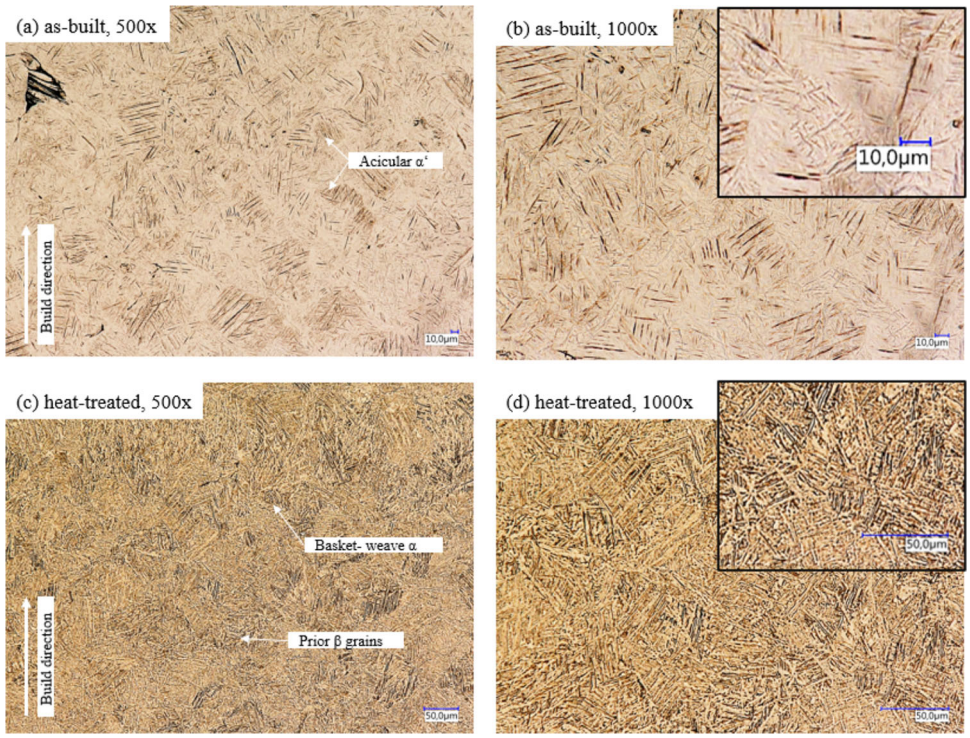

Fig. 3. Optical light microscope image of Ti-6Al-4V: (a) as-built, (b) as-built, close-up, (c) heat-treated, and (d) heat-treated, close-up.

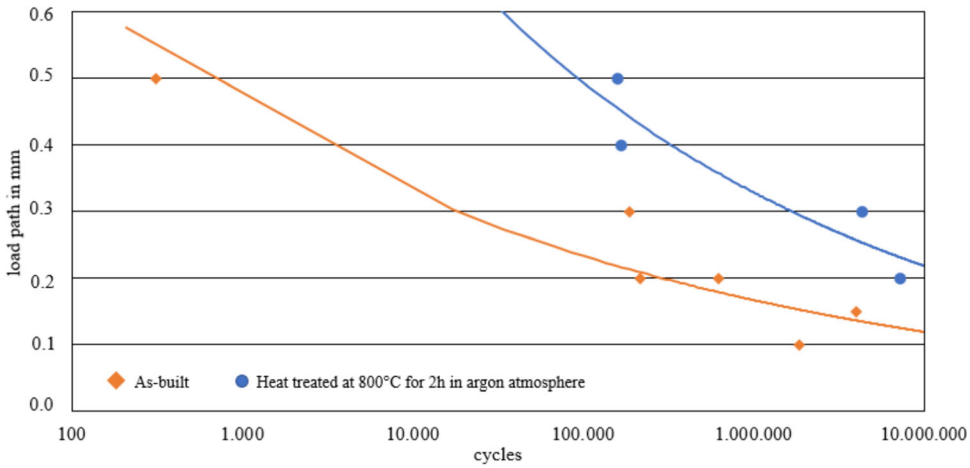

Fig. 4. Wöhler curve for as-built (orange) and heat-treated (blue) samples displacement-controlled at $f = 2$ Hz.

in the as-built condition at approximately 0.1 mm, while a subsequent heat treatment significantly increases the fatigue resistance to approximately 0.2 mm.

As demonstrated in the preceding analysis of microstructural images, the phase transformation that occurs during the process of heat treatment establishes a beneficial initial condition for dynamic loads. The decomposition of the α' phase into α lamellae, which are interspersed with β phase regions, facilitates the microstructure's capacity to respond to the induced load through a range of deformation mechanisms in response to loading. A significant deformation mechanism is twinning, leading to the formation of twin grain boundaries.[22] These twins serve to reduce the size of the grains, with the result that the dislocations induced by plastic deformation are accumulated at these twin boundaries at an early stage.[22] One consequence of increased twin formation is increased strain hardening. If further dislocations and twins are generated by plastic deformation, the orientation of the crystal lattice will change. This leads to a sharp increase in misorientation at the grain transitions. For uniaxial loading, the plane with a 45° orientation to the load axis is the plane on which the lowest stress is required to form dislocations. This factor is also referred to as the Schmid orientation factor. In

the case under consideration, the Schmid factor is also shifted to higher angles because of the increased misorientation at the grain transitions. However, if the stress is then reached at the angular ratio, crack nucleation occurs at the points of highest misorientation at the grain transitions, and continuous crack propagation occurs with further loading. This phenomenon has already been demonstrated in cp-titanium samples.[22]

The increasing work hardening is counteracted by the increasing ductility of the alloy. This is caused by the β-phase content in the alloy. These two factors play a decisive role in significantly improving the fatigue strength in the heat-treated condition of the samples. The martensitic as-built state has nearly no ductility, as the formation of a β-phase is linked to diffusion processes. The martensitic transformation, on the other hand, is diffusionless and prevents the formation of a β-phase. The fast cooling speeds lead to a constitutive undercooling of the melt, which reacts by forming a metastable network of Wittmanstaetten α' needles. This very fine microstructure can hardly form any dislocations. The ratio between yield strength and tensile strength leaves no scope for plastic deformation. If the elastic properties are exceeded, the sample fails almost immediately.

Residual Stresses of Additively Manufactured and Heat-Treated Specimens for Different States

Based on the process-related high cooling rates, the microstructure and the results of the Wöhler tests, additional RS measurements were carried out using X-ray diffraction (XRD) to better evaluate the influence of the microstructural stresses on the fatigue properties.

Three specimen states were examined: first, the stress state of the samples directly after production and removal from the laser powder bed fusion (LPBF) build platform. Secondly, measurements were taken after grinding and polishing the contact surface to the indenter in the dynamic test. Finally, RS data were collected again after the dynamic fatigue test. The same procedure was carried out for samples in the heat-treated state. The stress state is first determined in the heat-treated state and then after preparation. After the preparation stage, the heat-treated samples were examined once more for their RS state after the fatigue test. The graphs presented below show the measured normal RS in MPa in the top row and the shear in MPa in the bottom row.

The black numerals denote the state the samples at the time of measurement. Table II provides an overview of the existing states.

The colours are used to classify the measured RS. All compressive RS < -20 MPa are coloured green. All RS in a range between -20 and 20 MPa are coloured yellow and all tensile ones > 20 MPa are marked in red. The patterns of the bars are used for visual differentiation with the same colours. The sample orientations 0°, 45°, and 90° are always considered for all states. The orientation of the samples is set during the measurement via the rotation of the table and is shown schematically with the exposure strategy selected in the LPBF process in Fig. 5.

The RS states of the as-built specimens, shown in Fig. 6, show a clear discrepancy between the values in the normal stress region and the shear stress region. The analysis shows that the compressive RS directly after the manufacturing process are significantly higher in the normal stress region than in the shear stress region, and the investigation of the cooling conditions during the manufacture of the specimens shows that these are a significant factor in the formation of compressive RS. The rapid solidification of the micro-melts leads to a martensitic transformation associated with an increase in volume. This increase in volume manifests itself in the form of first order compressive RS.[16] For the 0° and 45° orientations, the subsequent preparation and dynamic testing reduce the RS in both the tensile and compressive planes. The range of shear RS at 45° is particularly significant. Here the production-induced compressive RS are transformed by the influence of the preparation into tensile RS, which are reduced by the dynamic test. The tendency to reduce the process-related RS can be attributed to several factors. These include the preparation, sample cooling, the grinding wheels and the rotational speed of the grinding wheels as well as the associated stock removal. High contact pressure and thus also plastic deformation and heating favour the formation of RS during preparation.[16] The formation of normal RS, which is particularly visible at 45° and 90°, may also be due to the direction of preparation, as the specimens were prepared in a 90° orientation.

As demonstrated in Fig. 7, the measurements were conducted under identical conditions after an additional heat treatment following manufacturing. The magnitude of the RS within the normal and shear range has undergone a substantial reduction. For the 0° and 45° orientations within the normal RS range, a continuous reduction in the compressive RS can be observed because of the preparation and dynamic testing steps, in alignment with the as-built condition. Although the orientation of this tendency is not directly evident, it is evident that no separate consideration is necessary after taking the displayed error bars into account; rather, the transformation of the compressive RS into tensile ones during the dynamic test is striking. When analysing the microstructure in consideration of the heat treatment condition, it becomes apparent that an increase in the β-phase fraction in the heat treatment condition leads to an increase in the alloy's ductility. This, in turn, leads to an increased number of dislocations being formed, which in turn

Table II. Overview of the tested conditions

State	Description
1	As-built
2	As-built after grinding and polishing the contact surface
3	As-built condition after the dynamic test
4	As-built heat-treated at 800°C for 2 h in Ar-atmosphere
5	As-built heat-treated after grinding and polishing the contact surface
6	As-built heat-treated condition after the dynamic test

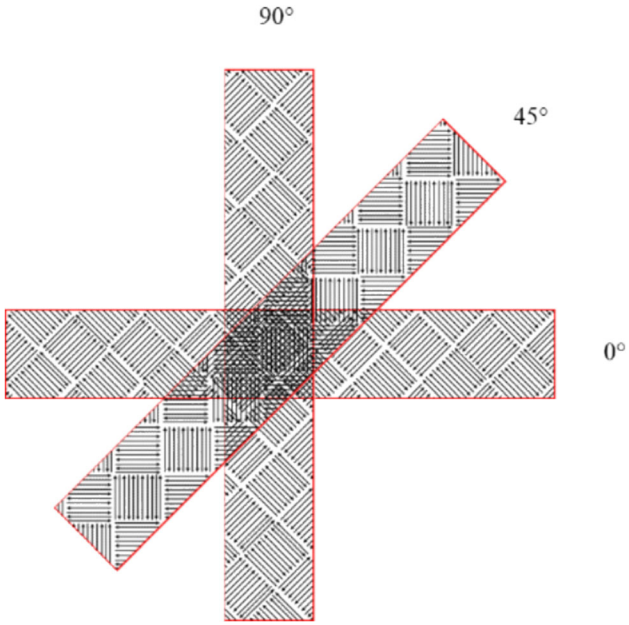

Fig. 5. Sample orientation for XRD measurement and scanning strategy in the LPBF process.

contributes to an increase in the residual stress components of third order.[16]

The evaluation of the measured shear RS post-preparation reveals the generation of compressive RS on the surface for all orientations. The preparation results in an increased dislocation density, particularly in the shear direction, due to the manual preparation of the specimens in the shear direction. Two significant effects occur during the dynamic test. On the one hand, dislocations are reduced; on the other hand, there is a reorientation at the texture level due to the dynamic load.[17] This can be recognized by converting the compressive RS into tensile ones.

Influence of Heat-Treatment on the Residual Stresses

In addition to the impact of the manufacturing process, preparation, and dynamic testing, the role of a heat treatment integrated within the manufacturing process must be substantiated. In numerous instances, the RS content can be mitigated through the thermal treatment of components, even after additive manufacturing.[16,23,24]

As illustrated in Fig. 8, the outcomes of the RS measurements are distilled into a direct comparison of the as-built (1) and heat-treated (4) states. While the compressive RS for the as-built samples are in a range between approximately − 140 MPa and − 250 MPa, the samples that were heat-treated in the as-built state only demonstrate very low compressive RS between approximately − 20 MPa and − 40 MPa. The shear stress range analysis further reveals that both states exhibit minimal stress components within the range of − 14 MPa to 5 MPa. This observation underscores the efficacy of heat treatment in inducing a substantial reduction in residual stresses.

The minimized RS are attributable to phase transformation, as previously demonstrated through metallographic analysis. During the heat treatment process, the energy input, manifested as heat, activates diffusion mechanisms, leading to phase decay. The metastable martensitic α' microstructure transforms into the two stable phases, α and β, under the influence of heat. Consequently, the microstructural stresses induced by the rapid solidification process can be substantially mitigated at heat treatment parameters of 800°C/2 h. The substantial measurement deviations observed in the as-built values, particularly in the domain of shear RS, can be attributed, at least in part, to the presence of a particularly fine martensitic microstructure in the as-built state. The peaks recorded for the individual orientations are subject to significant noise because of the presence of various diffractions. This effect is considerably reduced in the heat-treated microstructure because of its coarser basket-weave microstructure. Referring to the Wöhler curves shown in Fig. 4, the results documented there can also be reconciled. The RS reduced by phase transformation have a positive effect on the fatigue resistance of the samples, expressed in a doubling of the load path.

CONCLUSION

In summary, it can be posited that the residual stress state of additive samples is influenced by a variety of factors in different ways, including the manufacturing process, the associated cooling conditions, and the resulting microstructure formation. Furthermore, the residual stress state is influenced by additional factors of the post-treatment processes

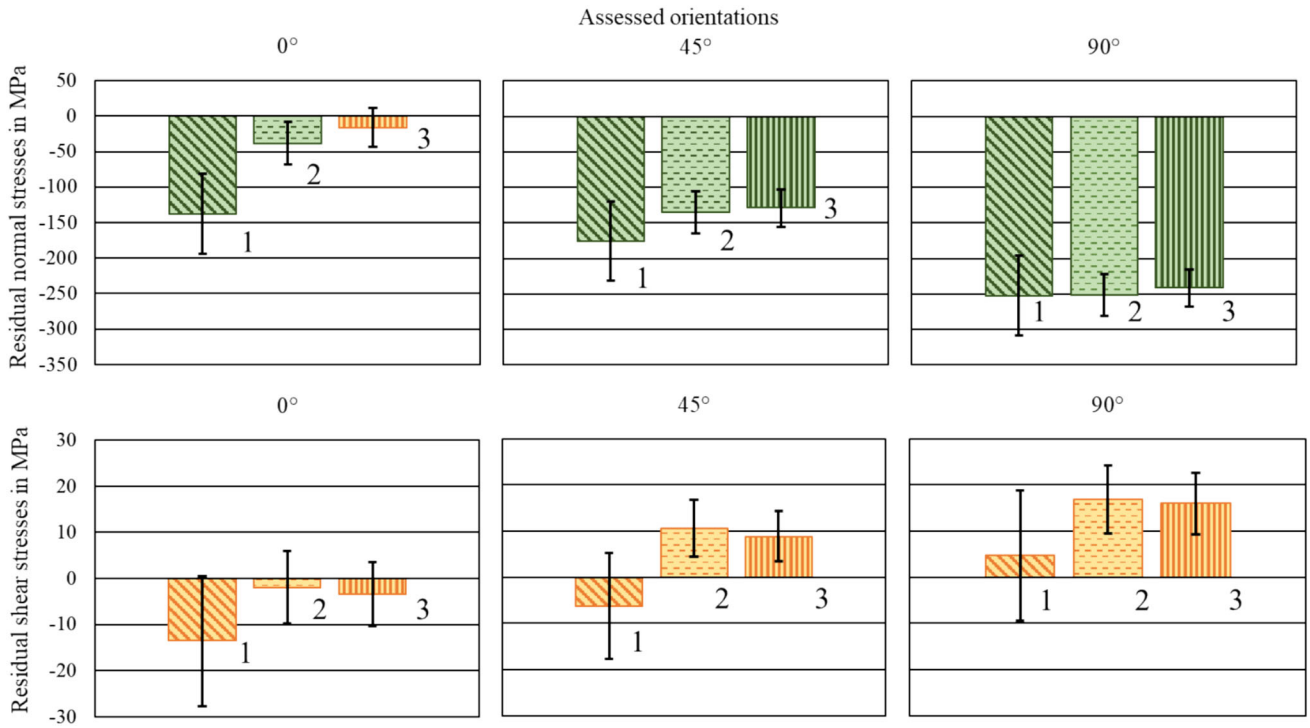

Fig. 6. Residual stress state in normal and shear stresses for the as-built condition: (1) as-built, (2), as-built ground and polished, (3) as-built ground, polished dynamically tested.

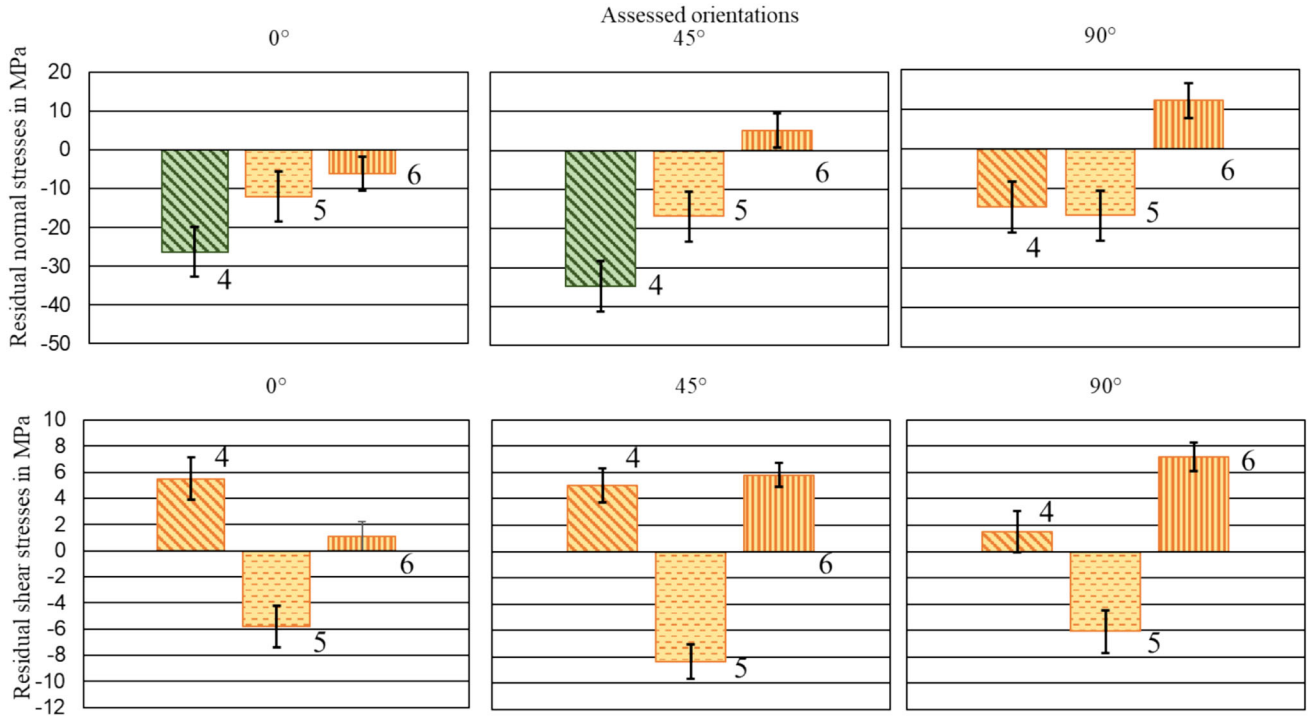

Fig. 7. Residual stress state in normal and shear stresses for the heat-treated condition: (4) as-built and heat-treated, (5) as-built, heat-treated, ground and polished, (6) as-built, heat-treated, ground, polished, and dynamically tested.

such as heat treatment, specimen preparation, and dynamic fatigue testing. The findings can be summarized as follows:

(1) The martensitic transformation of the melt into the α' caused by the high cooling rates produces a high residual stress state, charac-

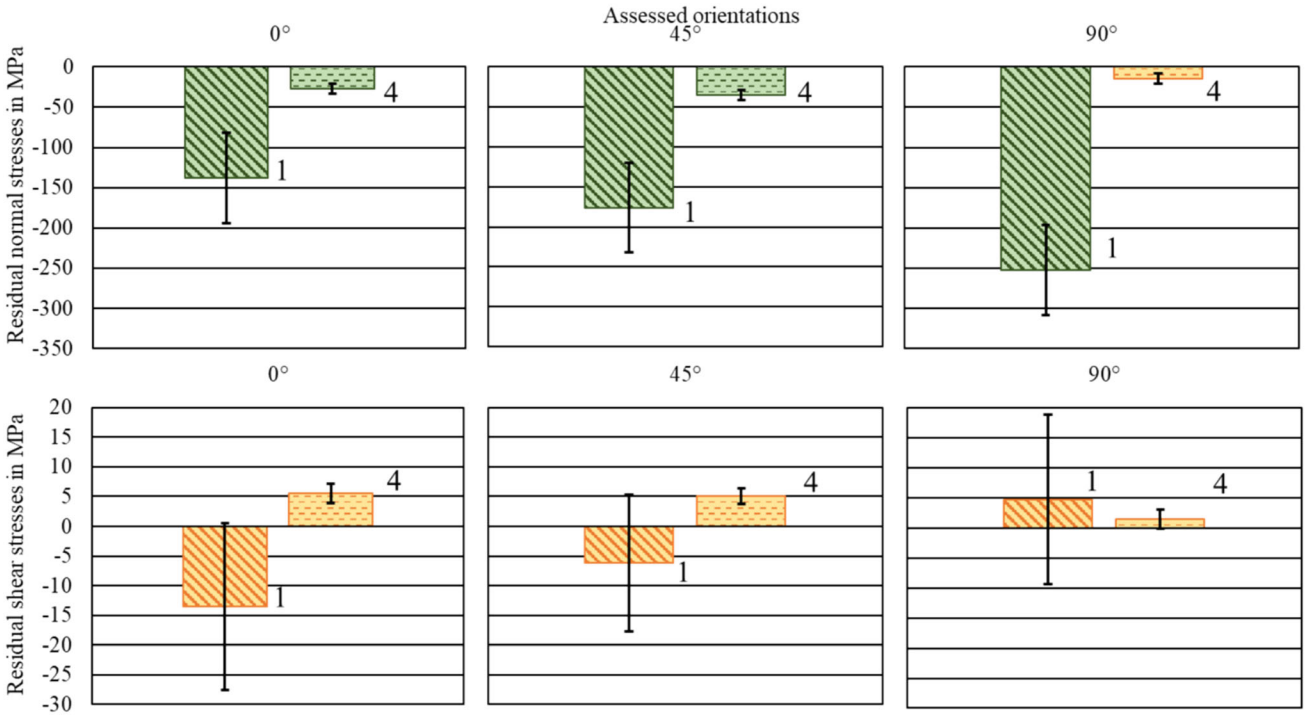

Fig. 8. Comparison of residual stress state in normal and shear stresses for the (1) as-built and (4) as-built and heat-treated states.

terized by low dislocation formation and early fatigue.

(2) The heat-treated state of the alloy exhibits significantly lower residual stresses because of the phase decomposition in $\alpha + \beta$.

(3) The twinning in α-phase and the increased ductility due to dislocation formation in the β-phase increase the fatigue strength of the samples.

(4) Preparing the contact surface by manual means before the dynamic tests is a more complex process due to the necessity of removing the support structures. In this instance, it is possible to induce residual compressive stresses in the shear direction (heat-treated); conversely, existing residual compressive stresses can also be reduced (as-built).

(5) For the as-built specimens, the dynamic test leads to a slight reduction in the existing residual compressive or shear stresses because of the brittle microstructural behaviour, which causes the specimen to fail before the residual stresses are further reduced.

(6) For the normal and shear residual stresses, the heat-treated specimens show a clear reduction in the compressive residual stresses and an induction of minor tensile residual stresses on the surface, which is possibly a result of the reduction in dislocations in combination with a reorientation of the preferred direction.

ACKNOWLEDGEMENTS

The authors acknowledge the financial support from the German Federal Ministry for Education and Research BMBF for this research (13FH5I09IA). Aesculap AG is gratefully acknowledged for supporting this research project.

FUNDING

Open Access funding enabled and organized by Projekt DEAL.

CONFLICT OF INTEREST

On behalf of all authors, the corresponding author states that there is no conflict of interest.

OPEN ACCESS

REFERENCES

1. B. Schramm, N. Rupp, L. Risse, J.-P. Brüggemann, A. Riemer, and H. Richard, *Additive Fertigung von Bauteilen und Strukturen*. https://doi.org/10.1007/978-3-658-17780-5_2 (2017).
2. VDI 3405:2024-12, Additive manufacturing processes, rapid manufacturing - Basics, definitions, processes, VDI-Gesellschaft Produktion und Logistik (2014).
3. DIN e.V. (Hrsg.) (DIN EN ISO/ASTM 52900:2022-03, 2022): DIN EN ISO/ASTM 52900:2022-03, Additive Fertigung - Grundlagen -Terminologie (ISO/ASTM 52900:2021); Deutsche Fassung EN_ISO/ASTM 52900:2021, Beuth Verlag GmbH, Berlin, (2022), https://doi.org/10.31030/3290011.
4. M. Schmid, Additive Fertigung mit Selektivem Lasersintern (SLS) -Prozess- und Werkstoffüberblick, Springer Vieweg, Wiesbaden, (2015), pp. 3–29, https://doi.org/10.1007/978-3-658-12289-8.
5. B. Dutta, and F.H. Froes, *Metal Powder Rep.* https://doi.org/10.1016/j.mprp.2016.12.062 (2017).
6. A. Liu, and Y.C. Shin, *Mater. Des.* https://doi.org/10.1016/j.matdes.2018.107552 (2019).
7. T. Töppel, B. Müller, K.P.J. Hoeren, and G. Witt, *Eigenspannungen und Verzug beim additiven Laser-Strahlschmelzen* (DVS-Verlag, Düsseldorf, Schweißen und Schneiden, 2016), pp176–186.
8. M. Biedermann, and M. Meboldt, *Konstruktion für die Additive Fertigung*. https://doi.org/10.1007/978-3-662-59058-4_3 (2020).
9. N. Bastola, M.P. Jahan, N. Rangasamy, and C.S. Rakurty, *Basel*. https://doi.org/10.3390/mi14071480 (2023).
10. R. Boillat-newport, S.P. Isanaka, J. Kelley, and F. Liou, *Basel*. https://doi.org/10.3390/ma17061333 (2024).
11. B.K. Nagesha, K. Vinodh, K.T. Amit, and B. Sanjay, *J. Manuf. Process.* https://doi.org/10.1016/j.jmapro.2021.04.020 (2021).
12. C. Ye, C. Zhang, J. Zhao, and Y. Dong, *ASM Int.* https://doi.org/10.1007/s11665-021-06021-7 (2021).
13. C. Leyens, and M. Peters, *Wiley-VCH Verlag GmbH & Co. KGaA*. https://doi.org/10.1002/3527602119 (2010).
14. D. Pede, M. Li, L. Virovac, T. Poleske, F. Balle, C. Müller, and M. Mozaffari-Jovein, *J. Mater. Res. Technol.* https://doi.org/10.1016/j.jmrt.2022.07.021 (2022).
15. G. Bergmann, F. Graichen, A. Rohlmann, A. Bender, B. Heinlein, G.N. Duda, M.O. Heller, and M.M. Morlock, *Biomed. Mater. Eng.* https://doi.org/10.3233/BME-2010-0616 (2010).
16. U. Wolfstieg, and E. Macherauch, *Chem. Ing. Tec.* https://doi.org/10.1002/cite.330451103 (1973).
17. A. Sarmast, J. Schubnell, J. Preußner, M. Hinterstein, and E. Carl, *J. Mater. Sci.* https://doi.org/10.1007/s10853-023-09069-z (2023).
18. G.S. Schajer, *Practical Residual Stress Measurement Methods* (Wiley, 2013) https://doi.org/10.1002/9781118402832.
19. T. Strauß, *Karlsruher Institut für Technologie (KIT) Institut für Angewandte Materialien – Werkstoffkunde (IAM-WK)*. https://doi.org/10.5445/IR/1000034516 (2013).
20. U. Zwicker, *Heidelberg*. https://doi.org/10.1007/978-3-642-80587-5_10 (1974).
21. M.J. Donachie, *ASM Int.* https://doi.org/10.31399/asm.tb.ttg2.9781627082693 (2000).
22. N. Bosh, *Technische Fakultät der Albert-Ludwig-Universität Freiburg im Breisgau*. https://doi.org/10.6094/UNIFR/193861 (2020).
23. S. Zhang, X. Lin, J. Chen, and W. Huang, *Rare Metal Mater. Eng.* https://doi.org/10.18154/RWTH-2024-00329 (2009).
24. D.G. Lee, Y. Choi, Effect of Heat Treatments on Fatigue Properties of Ti-6Al-4V Alloy Fabricated by EBM Additive Manufacturing, MATEC Web Conf. The 14th World Conference on Titanium, (20020), pp. 1–8, https://doi.org/10.1051/matecconf/202032103027.